Optical polarization tractography revealed significant fiber disarray in skeletal muscles of a mouse model for Duchenne muscular dystrophy

Y. Wang,[1] K. Zhang,[1] N. B. Wasala,[1] D. Duan,[1] and G. Yao[1,*]

[1]*Department of Bioengineering, [2]Department of Molecular Microbiology & Immunology University of Missouri, Columbia, MO 65211, USA*
[*]*yaog@missouri.edu*

Abstract: Optical polarization tractography (OPT) was recently developed to visualize tissue fiber architecture with cellular-level resolution and accuracy. In this study, we explored the feasibility of using OPT to study muscle disease in the mdx4cv mouse model of Duchenne muscular dystrophy. The freshly dissected tibialis anterior muscles of mdx4cv and normal mice were imaged. A "fiber disarray index" (FDI) was developed to quantify the myofiber disorganization. In necrotic muscle regions of the mdx4cv mice, the FDI was significantly elevated and can be used to segment the 3D necrotic regions for assessing the overall muscle damage. These results demonstrated the OPT's capability for imaging microscopic fiber alternations in muscle research.

References and links

1. A. E. H. Emery and F. Muntoni, *Duchenne Muscular Dystrophy* (Oxford University, 2003).
2. J.-H. Shin, C. Hakim, K. Zhang, and D. Duan, "Genotyping mdx, mdx3cv and mdx4cv mice by primer competition PCR," Muscle Nerve **43**, 283–286 (2011).
3. R. R. Scholten, S. Pillen, A. Verrips, and M. J. Zwarts, "Quantitative ultrasonography of skeletal muscles in children: normal values," Muscle Nerve **27**(6), 693–698 (2003).
4. J. F. Dunn and Y. Zaim-Wadghiri, "Quantitative magnetic resonance imaging of the mdx mouse model of Duchenne muscular dystrophy," Muscle Nerve **22**(10), 1367–1371 (1999).
5. B. R. Klyen, T. Shavlakadze, H. G. Radley-Crabb, M. D. Grounds, and D. D. Sampson, "Identification of muscle necrosis in the mdx mouse model of Duchenne muscular dystrophy using three-dimensional optical coherence tomography," J. Biomed. Opt. **16**(7), 076013 (2011).
6. R. M. Lovering, S. B. Shah, S. J. P. Pratt, W. Gong, and Y. Chen, "Architecture of healthy and dystrophic muscles detected by optical coherence tomography," Muscle Nerve **47**(4), 588–590 (2013).
7. B. R. Klyen, L. Scolaro, T. Shavlakadze, M. D. Grounds, and D. D. Sampson, "Optical coherence tomography can assess skeletal muscle tissue from mouse models of muscular dystrophy by parametric imaging of the attenuation coefficient," Biomed. Opt. Express **5**(4), 1217–1232 (2014).
8. X. Li, J. C. Ranasinghesagara, and G. Yao, "Polarization-sensitive reflectance imaging in skeletal muscle," Opt. Express **16**(13), 9927–9935 (2008).
9. J. J. Pasquesi, S. C. Schlachter, M. D. Boppart, E. Chaney, S. J. Kaufman, and S. A. Boppart, "In vivo detection of exercised-induced ultrastructural changes in genetically-altered murine skeletal muscle using polarization-sensitive optical coherence tomography," Opt. Express **14**(4), 1547–1556 (2006).
10. X. Yang, L. Chin, B. R. Klyen, T. Shavlakadze, R. A. McLaughlin, M. D. Grounds, and D. D. Sampson, "Quantitative assessment of muscle damage in the mdx mouse model of Duchenne muscular dystrophy using polarization-sensitive optical coherence tomography," J. Appl. Physiol. **115**(9), 1393–1401 (2013).
11. C. Fan and G. Yao, "Mapping local retardance in birefringent samples using polarization sensitive optical coherence tomography," Opt. Lett. **37**(9), 1415–1417 (2012).
12. C. Fan and G. Yao, "Mapping local optical axis in birefringent samples using polarization-sensitive optical coherence tomography," J. Biomed. Opt. **17**(11), 110501 (2012).
13. C. Fan and G. Yao, "Imaging myocardial fiber orientation using polarization sensitive optical coherence tomography," Biomed. Opt. Express **4**(3), 460–465 (2013).
14. Y. Wang and G. Yao, "Optical tractography of the mouse heart using polarization-sensitive optical coherence tomography," Biomed. Opt. Express **4**(11), 2540–2545 (2013).

15. Y. Wang, K. Zhang, N. B. Wasala, X. Yao, D. Duan, and G. Yao, "Histology validation of mapping depth-resolved cardiac fiber orientation in fresh mouse heart using optical polarization tractography," Biomed. Opt. Express **5**(8), 2843–2855 (2014).
16. S. Ponrartana, L. Ramos-Platt, T. A. Wren, H. H. Hu, T. G. Perkins, J. M. Chia, and V. Gilsanz, "Effectiveness of diffusion tensor imaging in assessing disease severity in Duchenne muscular dystrophy: preliminary study," Pediatr. Radiol. 1–8 (2014), doi:10.1007/s00247-014-3187-6.
17. C. Fan and G. Yao, "Full-range spectral domain Jones matrix optical coherence tomography using a single spectral camera," Opt. Express **20**(20), 22360–22371 (2012).
18. E. Götzinger, M. Pircher, W. Geitzenauer, C. Ahlers, B. Baumann, S. Michels, U. Schmidt-Erfurth, and C. K. Hitzenberger, "Retinal pigment epithelium segmentation by polarization sensitive optical coherence tomography," Opt. Express **16**(21), 16410–16422 (2008).

1. Introduction

Duchenne muscular dystrophy (DMD) is the most common and severe muscle disease caused by mutations in the dystrophin gene [1]. The absence of the dystrophin gene leads to body-wide muscle degeneration and necrosis. Most patients eventually die from respiratory and/or cardiac failure [1]. Animal models have been indispensable in our understanding of DMD and developing treatment. The mdx4cv mouse is a commonly used DMD animal model [2] where the dystrophin expression is abolished by a nonsense point mutation in exon 53.

Imaging techniques are important tools for evaluating muscle damage. Conventional histology can identify cellular level muscle damage. Unfortunately it only reveals a small region of interest and is not practical to provide three-dimensional (3D) information. Ultrasonography [3] and MRI [4] have been explored to evaluate muscle pathology. However, their resolution is too limited to resolve myofiber damage at the cellular level. Recently, optical coherence tomography (OCT) has emerged as a promising tool for high speed and high resolution skeletal muscle imaging [5–7]. Klyen et al. [5] found that damaged mdx muscle had a reduced OCT intensity and lower image contrast. Lovering et al. [6] observed atypical muscle architecture in the tibialis anterior muscles of mdx mice. Most recently Klyen et al. [7] reported that the optical attenuation coefficient extracted from depth-resolved OCT signals was significantly increased in necrotic muscle lesions [7].

As in any fibrous tissues, skeletal muscles show strong optical birefringence because the light experiences different optical refractive indices when propagating along and perpendicular to the muscle fiber [8]. Muscle damage disrupts the myofiber organization and thus can change the muscle birefringent properties. Tissue polarization properties can be imaged at high resolution using polarization-sensitive OCT (PSOCT), a functional extension of conventional OCT. Pasquesi et al. [9] explored the feasibility of using PSOCT to image mdx muscle and found that birefringence was significantly reduced in exercised mdx muscle. Yang et al. [10] recently constructed a novel "parametric image of birefringence" by calculating the slope of the phase retardation measured from 50 μm to 500 μm depth. Such calculated birefringence parameter was significantly smaller in necrotic regions [10].

In addition to the amount of birefringence (the difference between optical refractive indices parallel and perpendicular to the muscle fibers), the muscle fiber orientation (the "optical axis") is also an important parameter to characterize muscle birefringence. Because muscle necrosis disrupts the normal fiber structure, the optical axis would be altered accordingly. However, the value of the optical axis has not been explored for quantifying muscle lesions in the mdx mice model. Moreover, previous PSOCT studies on mdx muscle only imaged the "cumulative" polarization properties from the sample surface to a specific imaging depth, which makes it difficult to evaluate "local" lesions at a particular depth [11, 12]. The recently reported "parametric" birefringence imaging [10] only resulted in a 2D image instead of a true 3D polarization image. Therefore, new imaging strategies are needed to fully explore the potential of high resolution polarization imaging in skeletal muscle.

Optical polarization tractography (OPT) was recently developed for visualizing fiber orientation in tissue. It is based on Jones matrix implementation of PSOCT [13–15] to reconstruct the images of depth-resolved "local" optical axis. The obtained local optical axis

can be used to construct tissue tractographic images similar to those obtained in diffusion tensor MRI [16] but with cellular level resolution [15]. OPT has recently been applied for imaging cardiac myofiber architecture in the mouse heart [13-15]. In this paper, we demonstrated that OPT can effectively identify 3D skeletal muscle damage in freshly excised skeletal muscle samples of mdx4cv mice.

2. Method

2.1 Tissue processing

Four 7-m-old mdx4cv mice were imaged and four C57BL/6 mice were used as normal controls. The tibialis anterior (TA) muscle was excised and imaged immediately after euthanasia. After OPT imaging, the samples were fixed in 4% paraformaldehyde for at least 2 days. Then tissues were paraffin embedded, sectioned into slices of 5μm thick, and stained with hematoxylin and eosin (H & E). Histology images were then acquired using a Nikon Eclipse E800 microscope equipped with a QImaging RETIGA 1300 camera.

2.2 OPT imaging

OPT images were acquired using a single-camera spectral domain Jones matrix based PSOCT system. This imaging system has been described in details elsewhere [17]. Briefly, it is a bulk-optical OCT system using an 847.8 nm wavelength ($\Delta\lambda$ = 58.3 nm) superluminescent diode (SLD) as the light source. At the sample arm, a 5 × , f36 mm telecentric scan lens (LSM03-BB, Thorlabs, Newton, NJ) was used as the imaging objective. The optical power at the sample surface was 5.0 mW. Sample scanning was implemented using a 2D galvanometer scanner and covered an area of 8 × 8 mm^2 on the sample surface. At the detection arm, the interference spectra were acquired using a custom spectrometer equipped with a 1024-pixel line scan camera (AVIIVA SM2, e2v, Milpitas, CA). Images were acquired at a speed of 50k A-lines/sec. This imaging system had a measured lateral resolution of 12.4 μm and a measured axial resolution of <5.9 μm in tissue within a 1.5 mm imaging depth.

The polarization state of the incident light was modulated between right- and left-circular polarizations using an electric optical modulator [17]. At each incident polarization, the two orthogonally polarized signals (with horizontal and vertical polarization) were extracted separately from the interference spectra using two co-aligned reference beams with orthogonal polarization [13]. From these four signals, the Jones matrix at each pixel was then constructed [13,17]. The entire 3D image data set had a total 280 × 2000 × 1000 pixels along the A-, B- and C-scan directions and covered an imaging area of 1.1 × 8.0 × 8.0 mm^3 (A × B × C).

The local depth-resolved polarization properties including (slow) optical axis, retardance and diattenuation were computed from the 3D data set of Jones matrix at each image pixel. The retardance is defined as $\delta = 2\pi d\Delta n/\lambda$, where the "birefringence" Δn represents the difference in refractive indices along the orthogonal fast and slow optical axes; and d is the physical pathlength of the light. The birefringence can be derived from retardance as $\Delta n = \delta/(2\pi d/\lambda)$. The optical axis θ in our results was the "slow" optical axis representing the muscle fiber orientation in the *en face* (B-C) plane [13]. The diattenuation is defined as the different optical attenuation coefficient along the fast and slow optical axes. The local retardance and diattenuation were first calculated using similar matrix transformation [13]. Then a Jones calculus based iteration algorithm was applied to extract depth-resolved optical axis [11–13].

The final 3D data sets of local optical properties were resized using cubic spline interpolation to produce the same pixel size of 3.9 μm in A-, B-, and C-scan. The 3D image data was filtered using a 3 × 3 × 3 (pixel) median filter to improve the signal-to-noise ratio. When visualizing and analyzing the *en face* images, a 5 × 5 median filter was applied to further reduce noise. The tractographic image was constructed based on the local optical axis

using the streamline functionality in MATLAB and visualized using the 3DSlicer software as described in details previously [14, 15].

3. Results and discussions

Figure 1 shows representative cross-sectional and *en face* images of the freshly excised mdx4cv TA muscle. The upper inset of Fig. 1(d) shows the overall cross-sectional histology image (obtained using a $2 \times$ objective) with the corresponding OCT imaging area marked in blue dots. A small necrotic region located at the upper-right part of the muscle sample was marked with red dashed lines. The lower inset of Fig. 1(d) shows the high resolution images (obtained using a $40 \times$ objective) of the two small region-of-interest (ROI) marked in the $2 \times$ histology image. ROI #1 showed a region of non-damaged muscle; whereas ROI #2 showed a region of significant muscle necrosis and inflammation.
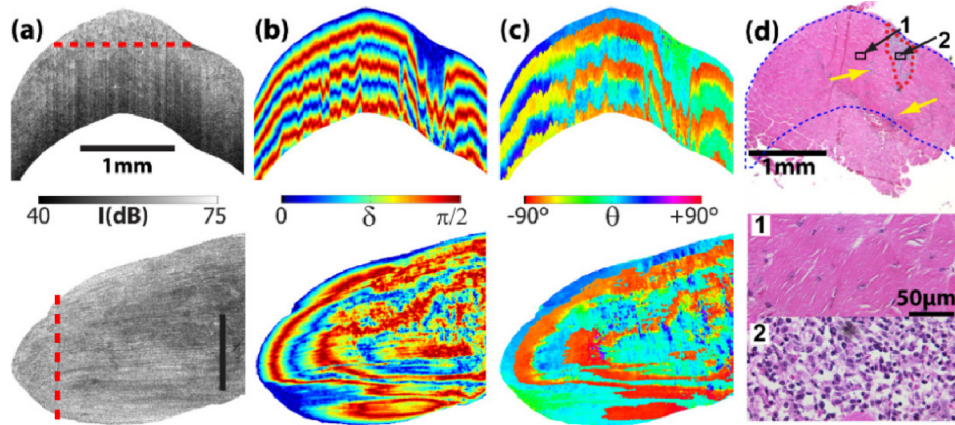

Fig. 1. Representative images of (a) OCT intensity, conventional cumulative (b) retardance and (c) optical axis of the mdx 4cv TA muscle. The upper row shows cross-sectional images and the lower row shows the *en face* images with the corresponding extraction locations marked with the red dashed lines. The size bars in (a) indicate 1 mm. (d) The corresponding histology image ($2 \times$) where the blue dots mark the OCT imaging region. The red dashed lines circles the main necrotic region. Yellow arrows indicate additional small necrotic regions observed in the HE histology image. Also shown are high resolution histology images ($40 \times$) of the two small region-of-interest as marked in the $2 \times$ histology image.

The muscle damage observed in histology (Fig. 1(d)) was barely detected in the OCT intensity image (Fig. 1(a)) except for a small low-intensity region very close to the surface in the cross-sectional image. However, the cross-sectional images of both cumulative retardance (Fig. 1(b)) and optical axis (Fig. 1(c)) showed altered patterns in areas corresponding to the muscle damage. The banded appearance in these images is caused by phase wrapping. The period of the banded pattern was longer in the damaged area than in the non-damaged areas. This indicated a smaller retardance value due to muscle damage as reported previously [9,10]. Both the cross-sectional and *en face* optical axis images are difficult to interpret because the cumulative optical axis in conventional PSOCT does not represent the true local fiber orientation [12]. In addition, the "banded" appearance in conventional retardance and optical axis images made it difficult to identify any small damaged areas (as indicated with yellow arrows in Fig. 1(d)) or the exact boundary of the lesion.

Figure 2 shows the OPT results including the local retardance (Fig. 2(a)) and local axis (Fig. 2(b)) images of the same sample position in Fig. 1. The necrotic muscle area revealed in histology (Fig. 1(d)) clearly had low local retardance values (indicated by darker blue color) in both the cross-sectional and *en face* images (Fig. 2(a)). The average birefringence was $(3.0 \pm 0.5) \times 10^{-4}$ in the damaged area vs. $(6.8 \pm 2.7) \times 10^{-4}$ in the surrounding non-damaged muscles. The images of local optical axis appeared to be relatively homogeneous. However a

closer examination indicated that the axes were much noisier in regions of muscle damage (Fig. 2(b)). This feature became more obvious in the fiber tractographic images (Fig. 2(c)). In regions with non-damaged muscle, the fiber bundles were long and well organized. However the fiber orientation was dramatically distorted in the damaged area.
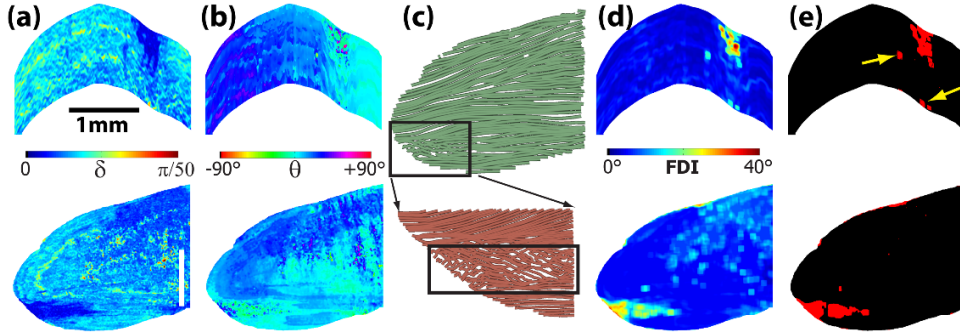

Fig. 2. The corresponding images of local (a) retardance and (b) optical axis at the same imaging locations as in Fig. 1. The size bars in (a) indicate 1 mm. (c) OPT fiber tractography obtained in the same *en face* plane as in Fig. 1. (d) The image of fiber disarray index. (e) Image segmentation using the disarray index (threshold = 16°). Yellow arrows indicate small necrotic regions corresponding to those marked in Fig. 1(d).

To quantify such variations in fiber orientation, a "fiber disarray index" (FDI) was constructed by calculating the standard deviation of the local optical axis within a small 3D evaluation window:

$$\mathbf{FDI} = \sqrt{\sum_{i,j,k=1}^{N} \left(\theta_{i,j,k} - \overline{\theta_{i,j,k}} \right)^2 / N^3}, \qquad (1)$$

where $\theta_{i,j,k}$ is the local axis at the pixel (i,j,k) and $\overline{\theta_{i,j,k}}$ is the average fiber orientation within the evaluation window. A fiber disarray image can be constructed using the FDI values calculated for each image pixel while "sliding" the evaluation windows over the entire 3D image volume. A similar procedure was previously applied to calculate depolarization in retinal pigment epithelium [18]. Figure 2(d) shows the image of the FDI calculated using a window size of N = 9 pixels ($35 \times 35 \times 35$ μm^3). Figure 2(e) shows the segmentation result based on the FDI using a threshold of 16° which was determined by analyzing the distribution of FDI in the entire imaging volume. The segmentation result showed an excellent agreement with the histology results including those small necrotic regions (Fig. 1(d)). The same good agreement was observed between other histology images and the corresponding OPT images obtained in the sample.

Figure 3 shows the 3D tractography of the TA muscle used in Figs. 1 and 2 (Fig. 3(a)) and another TA muscle from a different mdx4cv mouse (Fig. 3(b)). For the convenience of visualization, the damaged muscles were displayed in a different color from the non-damaged muscle. The damaged region showed substantial variations in fiber orientation and a fragmented appearance (Figs. 3(a) and 3(b)). Using a FDI threshold of 16°, the entire damaged muscle can be identified in the whole image volume (Figs. 3(c) and 3(d)). In addition to the FDI based segmentation, muscle damage can also be segmented using a birefringence threshold of 3.8×10^{-4} (Figs. 3(e) and 3(f)). Although the two segmentation results appeared similar, the high FDI in damaged muscle is likely caused by the disrupted fiber structure instead of a result of the coincided low birefringence. The low birefringence did not induce noticeable changes in signal-to-noise ratio. We previously obtained clear myofiber structure in heart muscles [14,15] with small birefringence values similar to that of the damaged skeletal muscle in this study. Using the ratio of pixel numbers in the damaged

and non-damaged muscle regions, the percentage of muscle damage can be calculated. The FDI based segmentation indicated that 4.7% muscle was damaged in one mouse (Fig. 3(a)); whereas 19.2% was damaged in the other (Fig. 3(b)). The local birefringence based segmentation gave very similar numbers of 4.2% and 19.4% in the mice shown in Figs. 3(a) and 3(b), respectively.
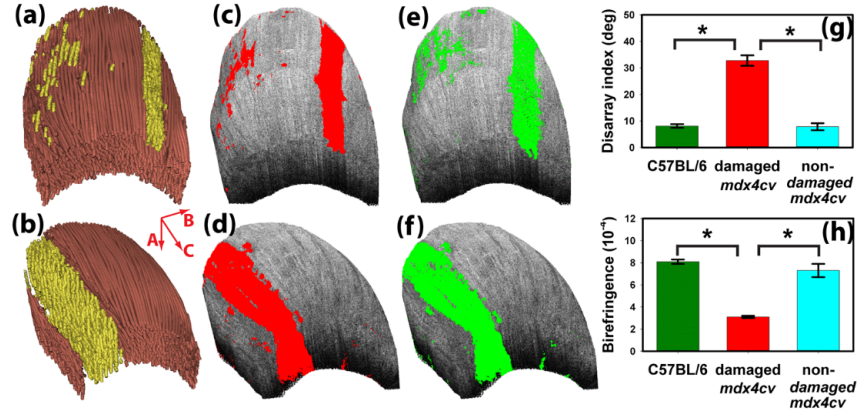

Fig. 3. (a, b) The 3D OPT images of two TA muscles from two different mdx4cv mice. The mouse used in (a), (c), and (e) was the same as shown in Figs. 1 and 2. The corresponding segmented results of muscle damage using fiber disarray index with a 16° threshold are shown in (b) and (d). (e) and (f) show the segmentation results using a birefringence threshold of 3.8 × 10^{-4}. Also shown are the statistical comparisons (*, $p<0.0001$) of the average (g) fiber disarray index and (h) local birefringence obtained in four mdx4cv mice and four C57BL/6 mice. Error bars represent standard deviations.

Figures 3(g) and 3(h) show a comparison of the group-averaged fiber disarray index and local birefringence obtained in normal C57BL/6 mice, the damaged and non-damaged regions of mdx4cv mice. One-way ANOVA with Bonferroni's post-hoc test confirmed that the fiber disarray index was significantly higher ($p<0.0001$) in damaged mdx4cv muscles (32.8° ± 2.0°) than in non-damaged mdx4cv muscles (7.8° ± 1.3°). Similarly, damaged mdx4cv muscles had a significantly smaller ($p<0.0001$) birefringence value of (3.1 × 10^{-4} ± 0.1 × 10^{-4}) than non-damaged mdx4cv muscles (7.3 × 10^{-4} ± 0.5 × 10^{-4}). These values are consistent with those reported in [10]. Both parameters appeared to have higher variations in non-damaged mdx4cv muscles than in muscles from normal C57BL/6 mice. However, no significant difference ($p>0.05$) was found in either the fiber disarray index or local birefringence between non-damaged mdx4cv muscles and muscles from normal C57BL/6 mice.

4. Conclusion

Optical polarization tractography (OPT) provides a unique tool for high resolution visualization of tissue fiber organization. In this study, we showed that OPT can successfully image muscle damages in freshly dissected TA muscle of the mdx4cv mice. OPT revealed significant fiber disorganization in regions corresponding to muscle necrosis as confirmed with histology. The local birefringence extracted in OPT was significantly lower in damaged muscle regions. Both fiber disarray index (FDI) and local birefringence can be used to segment the 3D necrotic regions and assess the overall muscle damage. These two parameters may be co-registered to further improve the segmentation. The results shown here demonstrated the great potential of OPT as a valuable imaging tool in muscle research.

Acknowledgment